

# Nodal signaling regulates endodermal cell motility and actin dynamics via Rac1 and Prex1

Stephanie Woo,<sup>1,2,3,4,5,6,7</sup> Michael P. Housley,<sup>1,2,3,4,5,6</sup> Orion D. Weiner,<sup>1,7</sup> and Didier Y.R. Stainier<sup>1,2,3,4,5,6,7</sup>

<sup>1</sup>Department of Biochemistry and Biophysics, <sup>2</sup>Developmental and Stem Cell Biology, <sup>3</sup>Institute for Human Genetics, <sup>4</sup>Liver Center, <sup>5</sup>Diabetes Center, <sup>6</sup>Institute for Regeneration Medicine, and <sup>7</sup>Cardiovascular Research Institute, University of California, San Francisco, San Francisco, CA 94158

**E**mbryo morphogenesis is driven by dynamic cell behaviors, including migration, that are coordinated with fate specification and differentiation, but how such coordination is achieved remains poorly understood. During zebrafish gastrulation, endodermal cells sequentially exhibit first random, nonpersistent migration followed by oriented, persistent migration and finally collective migration. Using a novel transgenic line that labels the endodermal actin cytoskeleton, we found that these stage-dependent changes in migratory behavior correlated with changes in actin dynamics. The dynamic actin and

random motility exhibited during early gastrulation were dependent on both Nodal and Rac1 signaling. We further identified the Rac-specific guanine nucleotide exchange factor Prex1 as a Nodal target and showed that it mediated Nodal-dependent random motility. Reducing Rac1 activity in endodermal cells caused them to bypass the random migration phase and aberrantly contribute to mesodermal tissues. Together, our results reveal a novel role for Nodal signaling in regulating actin dynamics and migration behavior, which are crucial for endodermal morphogenesis and cell fate decisions.

## Introduction

During the development of vertebrate organs, cells exhibit distinct morphologies and behaviors, such as cell migration, adhesion, and proliferation, that are indicative of their particular cell type and differentiation state. Although much work has been done to identify and characterize the signals that induce specific cell fates, how these developmental signals are translated into characteristic cellular behaviors is poorly understood.

Cell migration is important for numerous processes, including embryonic development, immune function, and wound healing, as well as the progression of diseases such as metastatic cancer. The mode of cell migration can be persistent, in which cells migrate in the same general direction over time, or nonpersistent, in which cells frequently change direction (Pankov et al., 2005; Petrie et al., 2009). Not only do different cell types exhibit different modes of migration, but the same cell may also change the way it migrates at different developmental stages (Bak and Fraser, 2003; Pézerson et al., 2008). These observations suggest that the type of migratory behavior is a marker of differentiation, but its significance is poorly understood.

Endodermal cells in the early zebrafish embryo exhibit multiple modes of migration and thus constitute an ideal model for investigating how different migratory behaviors are regulated. Just before gastrulation, high levels of Nodal signaling at the blastoderm margin induce endoderm specification (Stainier, 2002; Zorn and Wells, 2009). As gastrulation begins, endodermal cells undergo ingression and migrate between the yolk and epiblast. Initially, cells migrate in a random walk pattern, resulting in the dispersal of endodermal cells across the yolk surface in a discontinuous salt-and-pepper pattern (Pézeron et al., 2008). By 90% epiboly, endodermal cells begin a second phase of migration characterized by convergent movements toward the embryonic axis. Finally, these individual migratory cells must adhere together to ultimately form the epithelial lining of the gastrointestinal tract. These progressive changes in migration behavior are likely subject to tight regulation. However, although much work has been done to understand how developmental signaling molecules induce differential gene expression during endoderm differentiation and patterning (Stainier, 2002; Zorn and Wells, 2009), the downstream cellular responses, including migration, remain to be explored.

Correspondence to Stephanie Woo: stephanie.woo@ucsf.edu; or Didier Y.R. Stainier: didier.stainier@ucsf.edu

Abbreviations used in this paper: DN, dominant negative; GEF, guanine nucleotide exchange factor; MO, morpholino; PBD, p21-binding domain; ROI, region of interest.

© 2012 Woo et al. This article is distributed under the terms of an Attribution-Noncommercial-Share Alike-No Mirror Sites license for the first six months after the publication date (see <http://www.rupress.org/terms>). After six months it is available under a Creative Commons License (Attribution-Noncommercial-Share Alike 3.0 Unported license, as described at <http://creativecommons.org/licenses/by-nc-sa/3.0/>).

Supplemental Material can be found at:  
<http://jcb.rupress.org/content/suppl/2012/08/30/jcb.201203012.DC1.html>

Cell migration involves the complex rearrangement of the actin cytoskeleton, which is coordinated by numerous actin regulatory proteins (Rottner and Stradal, 2011). The Rho family of small GTPases, including RhoA, Rac1, and Cdc42, play several well-characterized roles in regulating actin dynamics during cell migration. For example, Cdc42 and Rac1 promote actin polymerization to drive membrane protrusion at the leading edge (Kozma et al., 1995; Wu et al., 2009), whereas RhoA induces actomyosin contraction, which provides the force necessary for cell translocation (Chrzanowska-Wodnicka and Burridge, 1996). The majority of studies investigating the molecular mechanisms underlying these actin dynamics have primarily used cells cultured on 2D or 3D substrates. However, it is known that cell migration can differ markedly *in vivo* (Yamada and Cukierman, 2007), but, until recently, it has been difficult to study subcellular actin dynamics within living organisms. In this study, we used a novel transgenic zebrafish line in which F-actin is fluorescently labeled specifically in endodermal cells. Using this line, we were able to track actin dynamics and cell motility at high resolution within the developing zebrafish embryo. We found that Nodal signaling can affect actin stability and retrograde flow in endodermal cells, which correlated with Nodal-dependent changes in cell migration. We further show that the effects of Nodal signaling on actin dynamics and cell migration are mediated by Rac1 and that Nodal signaling induces expression of the Rac activator Prex1. We found that similar to Nodal and Rac1, Prex1 is also required for the dynamic motility of endodermal cells and that it acts downstream of Nodal to drive random migration. Finally, we show that perturbing Rac1 activity in endodermal cells results in their aberrant contribution to mesodermal tissues, thereby revealing the importance of regulated cell motility to cell fate decisions.

## Results

### *Tg(sox17:GFP-UTRN)* expression labels F-actin in endodermal cells

To investigate the molecular mechanisms underlying endoderm migration *in vivo*, we generated a transgenic line in which the endoderm-specific *sox17* promoter drives expression of a fluorescent actin probe consisting of the F-actin-binding domain of Utrophin (Burkel et al., 2007) fused to GFP (*Tg(sox17:GFP-UTRN)*). *Tg(sox17:GFP-UTRN)* expression readily labels actin-rich structures *in vivo*, including lamellipodia, filopodia, retraction fibers, dorsal ruffles, actin bundles, and cleavage furrows of dividing cells (Fig. 1 and Videos 1–4). Cells often contained multiple sites of GFP-UTRN fluorescence, suggesting that actin polymerization is not restricted to a single leading edge. To examine actin dynamics during active migration, we imaged *Tg(sox17:GFP-UTRN)* gastrulae by time-lapse spinning-disk confocal microscopy (Videos 1 and 2). We observed that GFP-UTRN fluorescence rapidly accumulated in protrusive areas of cells, presumably a result of actin polymerization, and rapidly disappeared at sites of membrane retraction. Within the larger protrusions, we sometimes observed fluorescent particles streaming back toward the cell center, indicative of retrograde flow (arrow in Video 1). Thus, using this transgenic line,

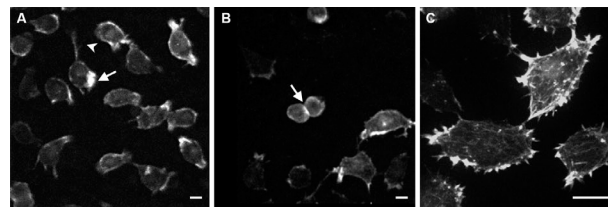


Figure 1. *Tg(sox17:GFP-UTRN)* expression labels actin-based structures in endodermal cells. (A–C) Images were taken from lateral marginal regions of gastrulating zebrafish embryos (6–9 h after fertilization). (A and B) Fluorescence from *Tg(sox17:GFP-UTRN)* expression accumulates in actin-based structures such as lamellipodia (arrow in A) and retraction fibers (arrowhead in A) as well as cytokinetic furrows (arrow in B). (C) More detailed actin organization including actin bundles can be seen at higher magnification. Bars, 10  $\mu$ m.

we can track actin rearrangements with high resolution in living embryos and gain further insights into the *in vivo* regulation of cytoskeletal dynamics.

### Endodermal cells exhibit progressive changes in migratory behavior and actin dynamics during gastrulation

A previous study has shown that endodermal cells undergo random migration during early gastrulation but switch to convergence movements in late gastrulation (Pézeron et al., 2008). We first confirmed that cells labeled by *Tg(sox17:GFP-UTRN)* expression exhibit similar migration behaviors. We quantified both the directional persistence of migration (defined as the ratio of net over total distance traveled) as well as the mean instantaneous velocity over 1-h intervals. During early stages (shield to 75% epiboly), cells migrated relatively randomly, although with a slight bias toward the dorsal side of the embryo (Fig. 2 [A and B] and Video 3). However, during late stages (90% epiboly to tailbud), endodermal cells moved with strong persistence in the dorsal direction, which was accompanied by a significant increase in migration velocity (Fig. 2, D and E). This switch from random to oriented migration was accompanied by a change in cell shape (Fig. 2 [F–H] and Video 3). In early stages, cells were mostly round with a few small lamellipodial protrusions (Fig. 2 F), but, by late stages, cells took on a flattened appearance with much broader lamellipodia (Fig. 2 G). By tail bud stage, the converging endodermal cells began to adhere to each other to form the endodermal sheet (Video 4).

By tracking GFP-UTRN fluorescence, we investigated the actin cytoskeletal rearrangements that occur during these changes in cell motility (Fig. 3 and Videos 1 and 2). First, we determined the dynamics of the actin cytoskeleton at early (70% epiboly) and late (90% epiboly) stages by measuring the persistence of GFP-UTRN fluorescence, focusing on the large fluorescent patches that often marked lamellipodia-like protrusions (Fig. 3, A and B). We found that these lamellipodia were relatively transient at 70% epiboly but were significantly more long lived at 90% epiboly (Fig. 3 C). This result suggests that the endodermal lamellipodia are more dynamic during early stages, which likely contributes to the ability of the cells to rapidly change migration direction. We also recorded the spatial orientation of lamellipodia within the cell with respect to the embryonic

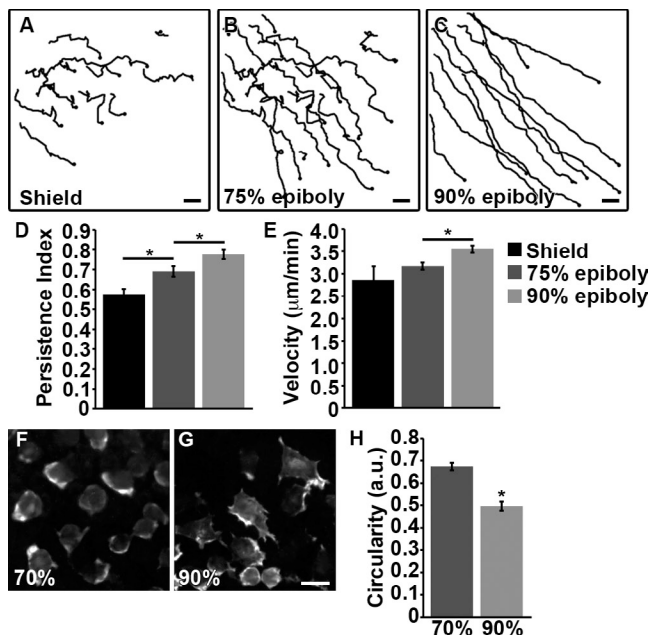


**Figure 2. Endodermal cells exhibit changes in migratory behavior and cell shape as embryos progress through gastrulation.** (A–C) Representative migration tracks over a 1-h period of endodermal cells at shield (6 h after fertilization; A), 75% epiboly (8 h after fertilization; B), and 90% epiboly (9 h after fertilization; C). Dorsal is to the right. Bars, 25 μm. (D and E) Quantification of migration persistence (D) and instantaneous velocity (E) shows that migration persistence and speed increase as gastrulation proceeds. Shield,  $n = 49$  cells; 75% epiboly,  $n = 74$  cells; 90% epiboly,  $n = 95$  cells. (F and G) Representative images of endodermal cells from *Tg(sox17:GFP-UTRN)* embryos at 70% epiboly (F) and 90% epiboly (G). (H) Quantification of circularity shows that cells are significantly more rounded at 70% epiboly. a.u., arbitrary units. 70% epiboly,  $n = 63$  cells; 90% epiboly,  $n = 66$  cells. All error bars represent SEM. \*,  $P < 0.05$ .

axes (dorsal, ventral, animal, or vegetal; Fig. 3 D). At 70% epiboly, lamellipodia oriented at similar frequencies toward the dorsal, ventral, or vegetal directions but were less likely to occur toward the animal pole. However, at 90% epiboly, lamellipodia formation was significantly more biased in the dorsal direction ( $P = 0.00163$  by  $\chi^2$  test). Thus, the preferential initiation and persistence of dorsally oriented actin polymerization likely underlie the dorsal-directed movement of endodermal cells at late stages.

A study of migratory cells in vitro has shown that the rate of retrograde flow decreases as protrusion persistence increases (Lim et al., 2010). Therefore, we used kymography (Batchelder et al., 2011) to determine whether retrograde flow within protrusions varied from early to late stages (Fig. 3, E–I). We found that the rate of retrograde flow within endodermal cells was significantly faster during early compared with late stages (Fig. 3 I), correlating with the shift from random to oriented migration.

#### Nodal signaling promotes random migration and actin dynamics during early stages

A study has reported that the dorsally oriented migration of endodermal cells during late gastrulation depends on the chemokine Cxcl12b and its receptor Cxcr4a (Mizoguchi et al., 2008). In contrast, the mechanisms controlling early random migration

are less clear, although one study suggests that Nodal signaling may promote random migration of mesendodermal cells (Pézeron et al., 2008). Nodal is a member of the TGF- $\beta$  superfamily of signaling proteins that is required for the specification of endoderm and mesoderm (Feldman et al., 1998; Stainier, 2002). Classically, the role of Nodal signaling during endoderm development has been to induce the expression of endoderm-specific transcription factor genes (Alexander and Stainier, 1999; Reiter et al., 2001; Poulain and Lepage, 2002; Stainier, 2002; Zorn and Wells, 2009). To determine whether Nodal signaling regulates the migration of endodermal cells in addition to its role in endodermal fate specification, we treated *Tg(sox17:GFP-UTRN)* embryos with the Nodal receptor/Alk4/5/7 inhibitor SB-505124 (Fig. 4; Hagos and Dougan, 2007). To focus on events subsequent to endoderm specification, inhibitor treatment started at 5 h after fertilization, which does not appear to interfere with the onset of endodermal marker gene expression (Fig. S1, A–D). We found that treatment with 50 μM SB-505124 significantly slowed migration velocity and increased migration persistence at early stages (70% epiboly) compared with DMSO-treated control (Fig. 4 [A–D] and Video 5). Nodal receptor inhibition also induced changes in actin dynamics. In particular, we found that SB-505124 treatment significantly increased lamellipodia lifetime and slowed the rate of retrograde flow (Fig. 4, E–J). However, we did not detect any directional bias in lamellipodia formation (unpublished data), suggesting that although Nodal inhibition can promote migration persistence, it likely does not provide guidance information.

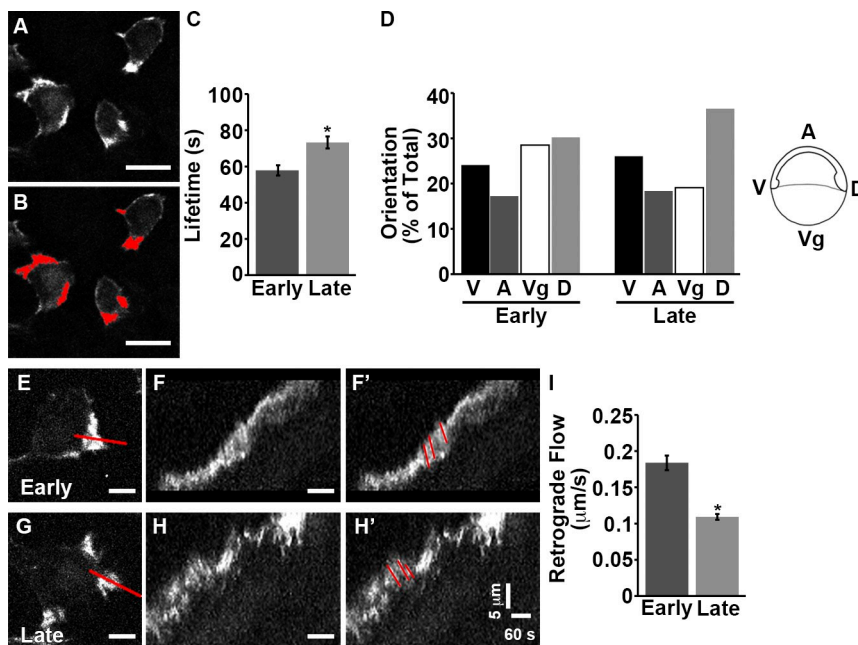
#### Nodal signaling promotes Rac1 activity in endodermal cells

Our results suggest that Nodal signaling can regulate actin dynamics, but there are no known cytoskeletal regulators in the Nodal signaling pathway. To identify a link between Nodal and the actin cytoskeleton, we focused on the Rho family GTPase Rac1 as a candidate. Rac1 has well-characterized roles in many aspects of cell migration, including promoting actin polymerization and lamellipodia formation (Ridley et al., 1992). The characteristics of endodermal cells during early gastrulation—in particular, weak directionality and short-lived, nonoriented protrusions—are strikingly similar to cells expressing constitutively active forms of Rac1 (Pankov et al., 2005; Woo and Gomez, 2006). Moreover, expression levels of Rac1 were shown to be sufficient to modulate the migration persistence of fibroblasts in vitro, with high levels promoting random migration and low levels facilitating persistent migration (Pankov et al., 2005).

First, we determined whether Rac1 was required for early random migration by overexpressing dominant-negative (DN) Rac1 in *Tg(sox17:GFP-UTRN)* embryos. Injection of large amounts of DN Rac1 mRNA (10 pg) resulted in cessation of all cell movements (unpublished data). However, a low dose of DN Rac1 mRNA (2 pg) only moderately inhibited endodermal migration speed but significantly increased migration persistence at 70% epiboly, similar to what was observed with Nodal receptor inhibition (Fig. 4, K–N). This low dose of DN Rac1 expression did not appear to affect expression of the endodermal

**Figure 3. Actin dynamics within endodermal cells change from early to late gastrulation.** (A and B) Actin dynamics were analyzed by tracking lamellipodia through accumulations in GFP-UTRN fluorescence. Representative lamellipodia are highlighted in red in B from the cells in A. Bars, 25  $\mu\text{m}$ .

(C) Lamellipodial lifetime increases during late gastrulation. Early (70% epiboly),  $n = 523$  lamellipodia from 45 cells; late (90% epiboly),  $n = 665$  lamellipodia from 77 cells. (D) Orientation of lamellipodia formation with respect to the embryonic axes. V, ventral; A, animal; Vg, vegetal; D, dorsal. Lamellipodia formation is biased toward the dorsal direction during late gastrulation ( $P = 0.00163$  by  $\chi^2$  test). Early (70% epiboly),  $n = 45$  cells; late (90% epiboly),  $n = 77$  cells from two independent experiments. (E–I) Analysis of retrograde flow. Kymographs in F and H were generated along the red lines shown in E and G, respectively. Time is plotted horizontally, and the direction of membrane protrusion is oriented toward the top of the images. Red lines in F' and H' highlight retrograde-moving actin structures, which form streaks in the kymographs. The slope of these streaks was used to calculate the rate of retrograde flow (I), which decreases in late gastrulation. Early (70% epiboly),  $n = 12$  cells; late (90% epiboly),  $n = 15$  cells. Bars: (E–H) 10  $\mu\text{m}$ ; (F' and H') 5  $\mu\text{m}$ . All error bars represent SEM. \*,  $P < 0.05$ .

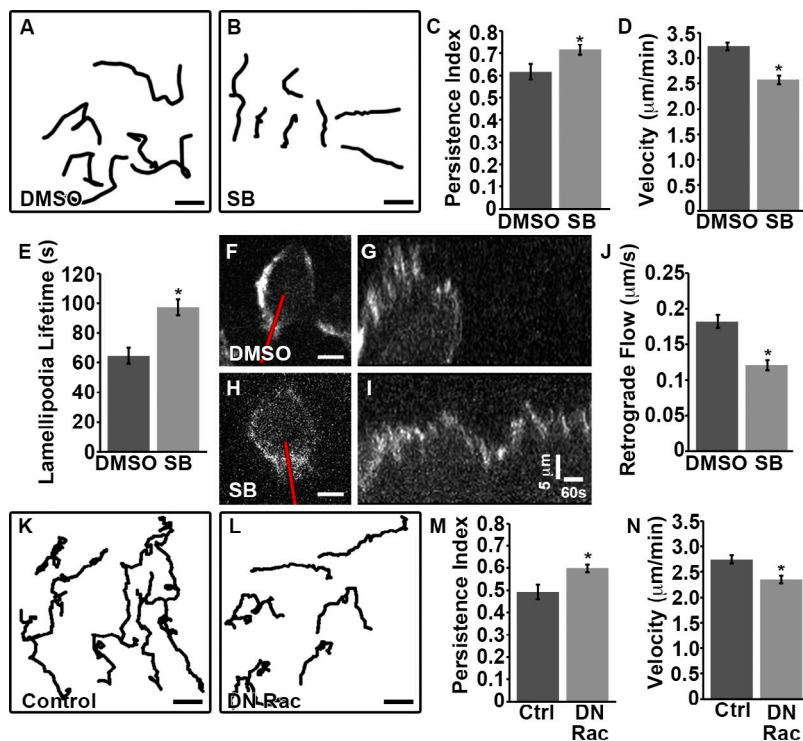


marker genes *sox17* and *sox32* (Fig. S1, E–H), suggesting that the effects on endodermal motility were not a result of mis-specification. To determine whether Rac1 was required cell autonomously within endodermal cells to promote dynamic migration, we performed cell transplantation experiments. Donor endodermal cells were generated by overexpression of *sox32* either alone or combined with DN Rac1. Cells were transplanted into wild-type host embryos at 4–5 h after fertilization, and cell

motility was assessed starting at 70% epiboly. Importantly, transplanted *sox32*-overexpressing cells display biphasic migration behaviors similar to those of endogenous endodermal cells, switching from random to persistent migration between early/mid and late gastrulation (Fig. S2, A–D). These cells also undergo the corresponding changes in cell shape (Fig. S2, E and F). However, when transplanted cells coexpressed DN Rac1, we found that directional persistence significantly increased during

**Figure 4. Cell migration and actin dynamics during early gastrulation depend on Nodal and Rac1 signaling.** (A and B) Representative migration tracks over a 1-h period from embryos treated with DMSO carrier (A) and 50  $\mu\text{M}$  Nodal receptor inhibitor SB-505124 (SB; B). Dorsal is to the right. Bars, 25  $\mu\text{m}$ .

(C and D) Quantification of migration persistence and instantaneous velocity shows that Nodal inhibition leads to significantly increased migration persistence and reduced migration velocity. DMSO,  $n = 74$  cells; SB-505124,  $n = 48$  cells. (E) Nodal inhibition increases lamellipodial lifetime. DMSO,  $n = 191$  lamellipodia from 28 cells; SB-505124,  $n = 324$  lamellipodia from 46 cells. (F–J) Nodal inhibition slows retrograde flow. Kymographs in G and I were generated along the red lines shown in F and H, respectively. Time is plotted horizontally, and the direction of membrane protrusion is oriented toward the top of the images. Bars: (F and H) 10  $\mu\text{m}$ ; (G and I) 5  $\mu\text{m}$ . The rate of the retrograde flow is quantified in J. DMSO,  $n = 9$  cells; SB-505124,  $n = 5$  cells. (K and L) Representative migration tracks over a 1-h period from control embryos (K) and embryos expressing DN Rac1 (L). Bars, 25  $\mu\text{m}$ . (M and N) Quantification of migration persistence and instantaneous velocity from control (Ctrl) embryos and embryos expressing DN Rac1. Loss of Rac1 activity significantly increases migration persistence and moderately reduces migration velocity. Control,  $n = 76$  cells; DN Rac1,  $n = 98$  cells. All error bars represent SEM. \*,  $P < 0.05$ .



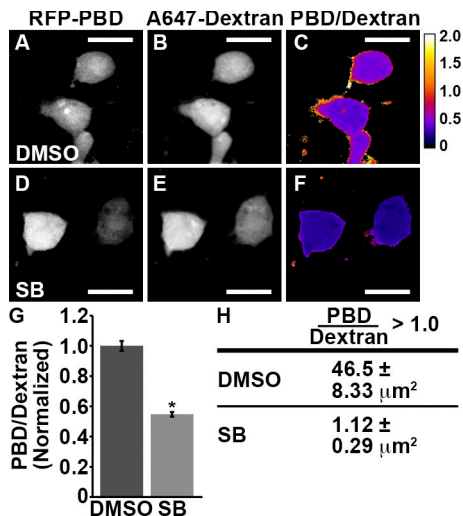


**Figure 5. Nodal signaling regulates Rac1 activity.** (A–F) Visualization of Rac1 activity in embryos treated with DMSO (A–C) and SB-505124 (SB; D–F). A fluorescent Rac1 probe, RFP-PBD, was expressed in endodermal cells (A and D). Cells were colabeled with fluorescent dextran (B and E) as a volume marker. Rac1 activity was determined by generating ratiometric images between the RFP-PBD and dextran signals and was pseudocolored based on ratio value (C and F). Warmer colors indicate enrichment of PBD relative to dextran. Bars, 10  $\mu\text{m}$ . (G) Quantification of the mean ratio of PBD to dextran indicates that Nodal inhibition reduces Rac1 activity. DMSO,  $n = 121$  cells; SB-505124,  $n = 125$  cells. All error bars represent SEM. \*,  $P < 0.05$ . (H) Measurement of the size of cell regions where the PBD/dextran ratio is  $>1.0$ . Area of Rac1 activation is dramatically reduced upon Nodal inhibition.

early stages, whereas migration velocity was significantly slower, suggesting that Rac1 acts cell autonomously to regulate endoderm migration (Fig. S2, G–J).

Next, we determined whether Nodal signaling regulates Rac1 activity (Fig. 5). To visualize Rac1 activity, we expressed a fluorescent probe consisting of the Rac1-binding domain of p21-activated kinase tagged to an RFP (RFP-p21-binding domain [PBD]; Srinivasan et al., 2003; Miller and Bement, 2009). Because detection of RFP-PBD fluorescence is facilitated by mosaic expression, we transplanted small groups of RFP-PBD-expressing endodermal cells into unlabeled hosts. To control for variation in cell size or shape, donor cells were colabeled with Alexa Fluor 647-conjugated 10,000-molecular weight dextran (A647-dextran) as a volume marker, and Rac1 activity was determined as the ratio of the RFP-PBD signal relative to the A647-dextran signal. We found that active Rac1 was enriched along the cell periphery and concentrated within actively protruding areas of endodermal cells (Fig. 5 C and Video 6). This observation is consistent with previous in vitro studies showing that active Rac1 localizes to the cell membrane and leading edge (Kraynov et al., 2000; Srinivasan et al., 2003). Treatment with SB-505124 resulted in a global decrease in active Rac1 compared with DMSO-treated control (Fig. 5 G). We also measured the area of regions within cells in which the ratio of RFP-PBD to A647-dextran was  $>1.0$  (Fig. 5 H), as these regions often corresponded to membrane protrusions. These regions were significantly reduced in size upon inhibitor treatment, suggesting that active Rac1 was no longer differentially

localized to membrane protrusions. Collectively, these results suggest that Nodal signaling promotes Rac1 activation to induce membrane protrusions.

Using the same RFP-PBD assay, we also investigated whether a drop in Rac1 activity accompanies the switch from random to persistent migration in wild-type gastrulae (Fig. S4 I). Surprisingly, we found that levels of Rac1 significantly increased during late gastrulation. One likely explanation is the onset of Cxcl12a–Cxcr4 chemokine signaling at this stage (Mizoguchi et al., 2008), which is known to activate Rac1 (Xu et al., 2012).

#### The Rac-guanine nucleotide exchange factor (GEF) *prex1* is a Nodal target gene and is required for random migration

Small GTPases such as Rac1 are activated by GEFs, which promote the dissociation of GDP, allowing GTP to bind. TGF- $\beta$ 1 has been shown to induce the expression of the Rho-GEF *NET1*, leading to increased RhoA activity and actin stress fiber formation (Shen et al., 2001). Therefore, we hypothesized that Nodal might similarly regulate expression of a Rac-GEF to control Rac1 activity. To identify endodermally enriched Nodal target genes, we performed microarray analysis using *Tg(sox17:GFP)* embryos treated with SB-505124 to inhibit Nodal signaling or overexpressing a constitutively active form of the *acvr1b* Nodal receptor (*taram-a\**). Of the genes identified, three were Rac-specific GEFs: *arhgef25b*, *prex1*, and *tiam1* (Fig. S3 A). We verified these candidates by quantitative real-time PCR and found that only *prex1* expression was consistently Nodal responsive (Figs. 6 A and S3 B). When embryos were treated with SB-505124, *prex1* expression was down-regulated  $2.8 \pm 0.45$  fold compared with DMSO-treated control. Correspondingly, when Nodal signaling was activated by expression of the constitutively active receptor *taram-a\**, *prex1* expression increased  $2.85 \pm 0.5$  fold compared with that in embryos expressing a control RNA.

*Prex1* was initially identified in neutrophils as a protein required for phosphatidylinositol (3,4,5)-trisphosphate (PIP<sub>3</sub>)-induced Rac activation (Welch et al., 2002). It consists of a RhoGEF domain, a pleckstrin homology domain, two DEP (dishevelled, Egl-10, and pleckstrin) domains, two PDZ domains, and a C-terminal region with significant similarity to inositol polyphosphate-4-phosphatase but that is apparently catalytically inactive. *Prex1* is synergistically activated by PIP<sub>3</sub> and G $\beta\gamma$  (Welch et al., 2002; Barber et al., 2007; Zhao et al., 2007) and is important for neutrophil function (Welch et al., 2005), neurite formation (Waters et al., 2008), and motility of breast cancer cells (Sosa et al., 2010). By in situ hybridization, we found that at 70% epiboly, when endodermal cells are undergoing random migration, *prex1* appears to be most highly expressed within the endoderm (Fig. 6 B).

We determined whether *Prex1* functions as a Rac-GEF in zebrafish endodermal cells by examining the effects of morpholino (MO)-mediated knockdown of *Prex1* on Rac1 activity (Fig. 6, C–E). Using the same aforementioned PBD fluorescence assay, we found that *Prex1* knockdown resulted in a significant decrease in Rac1 activity (Fig. 6 E). We also examined the

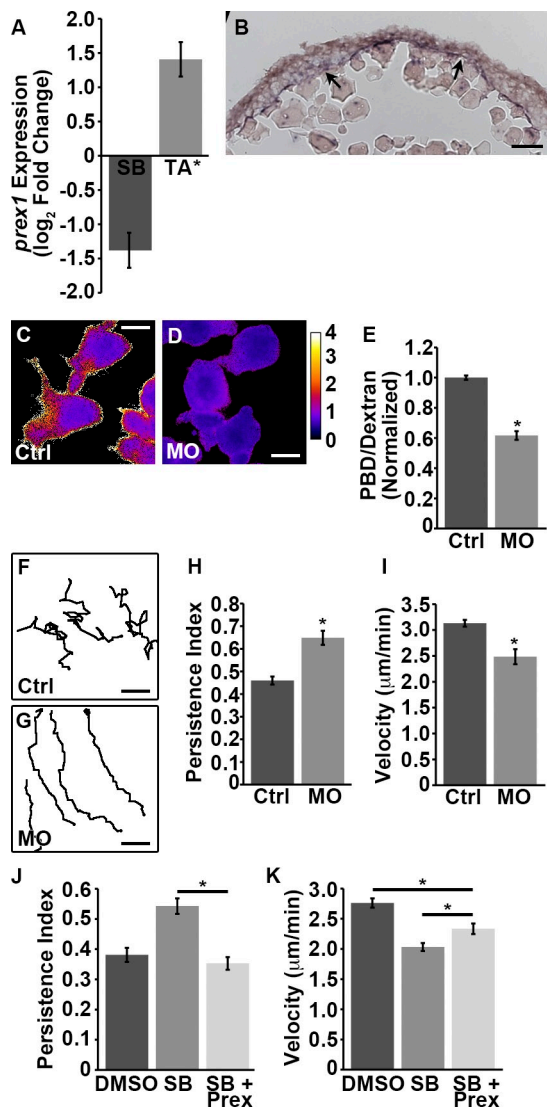


**Figure 6. *prex1* is a target of Nodal signaling, promotes Rac1 activity, and regulates endodermal cell motility.** (A) Expression of *prex1* was measured by real-time quantitative PCR. Inhibition of Nodal signaling by SB-505124 treatment (SB) down-regulated *prex1* expression (normalized to DMSO-treated controls), and overactivation of the Nodal pathway by expression of taram-A\* (TA\*) increased *prex1* expression (normalized to control embryos expressing mCherry). The data shown are mean fold changes from six independent experiments. (B) Section through an embryo at 70% epiboly processed for *prex1* in situ hybridization. *prex1* appears to be enriched within the endodermal layer (arrows). Bar, 25  $\mu$ m. (C and D) Representative ratiometric images of control (Ctrl; C) and Prex1 MO-injected (D) cells expressing RFP-PBD and colabeled with fluorescent dextran. Images are pseudocolored based on ratio value. Warmer colors indicate enrichment of PBD relative to dextran. Bars, 10  $\mu$ m. (E) Quantification of the mean ratio of PBD to dextran indicates that Prex1 knockdown reduces Rac1 activity. Control,  $n = 124$  cells; MO,  $n = 70$  cells. (F and G) Representative migration tracks over a 1-h period from control (F) and Prex1 MO-injected (G) embryos. Dorsal is to the right. Bars, 25  $\mu$ m. (H and I) Quantification of migration persistence (H) and instantaneous velocity (I) from control and Prex1 MO-injected embryos. Prex1 knockdown significantly increased migration persistence and moderately reduced migration velocity. Control,  $n = 80$  cells; MO,  $n = 33$  cells. (J and K) Overexpressing Prex1 can rescue random migration (J) and partially rescue migration velocity (K) in embryos treated with the Nodal inhibitor SB-505124. DMSO,  $n = 44$  cells; SB-505124,  $n = 34$  cells; SB-505124 + Prex,  $n = 52$  cells. All error bars represent SEM. \*,  $P < 0.05$ .

effects of Prex1 on endodermal motility during early stages by injecting Prex1 MO into *Tg(sox17:GFP-UTRN)* embryos (Fig. 6, F–I). In these MO-injected embryos, we observed some GFP-UTRN-labeled cells positioned in the cell layers away from the yolk surface (Video 9), suggesting that reduction in Prex1 levels leads to defects in internalization or other epiboly movements. Notably, we did not observe these effects with DN Rac1 expression. As these superficial cells appeared rounded and immobile, we excluded them from subsequent analysis and restricted our measurements to the cells that were positioned at the yolk surface. Similar to the observations with both Nodal inhibition and DN Rac1 expression, we found that Prex1 knockdown significantly increased migration persistence (Fig. 6 H) and decreased migration velocity (Fig. 6 I).

Next, we examined whether Prex1 acts downstream of Nodal to promote random migration of endodermal cells by determining whether overexpressing Prex1 was able to rescue the effects of Nodal inhibition on cell motility (Fig. 6, J and K). Embryos injected with 500 pg Prex1 mRNA or an equivalent amount of mCherry mRNA as a control were treated with 50  $\mu$ M SB-505124 at 5 h after fertilization, and cell motility was assessed at 7 h after fertilization. As we previously observed, control-injected embryos treated with Nodal inhibitor exhibited increased directional persistence and decreased migration velocity. Overexpression of Prex1 rescued the effects on directionality and partially rescued the effects on migration velocity, suggesting that Prex1 at least partially mediates signaling downstream of Nodal to control endodermal cell motility.

All together, these results suggest that *prex1* is an endodermally expressed Nodal target gene that activates Rac1 and mediates the Nodal-dependent dynamic motility of endodermal cells.

### Random migration is required to maintain endodermal identity

It is not clear how an initial phase of random migration contributes to subsequent steps of endodermal morphogenesis. To address this question, we expressed low levels of DN Rac1 to bypass the random migration phase and promote precocious persistent migration and then assessed the effects on later stages of endoderm development (Fig. 7). Control endodermal donor cells labeled by *Tg(sox17:dsRed)* expression were transplanted together with DN Rac1-expressing cells labeled by *Tg(sox17:GFP)* expression into unlabeled wild-type hosts before gastrulation (4–5 h after fertilization). The distribution of GFP- and dsRed-labeled cells was then assessed at 22–24 h after fertilization. We found that the majority of both control and Rac1-deficient cells were located within the gut tube and pharyngeal endoderm (Fig. 7, A–D). However, a significant proportion of cells expressing DN Rac1 was found within mesodermal tissues such as the somites and notochord (arrows in Fig. 7 [A, C, E, and F]). The percentage of cells residing in such nonendodermal positions was significantly higher among DN Rac1-expressing donor-derived tissue than control (Fig. 7 G). Intriguingly, these cells were still *Tg(sox17:GFP)* positive but exhibited the characteristic cell shapes and expressed molecular markers of the

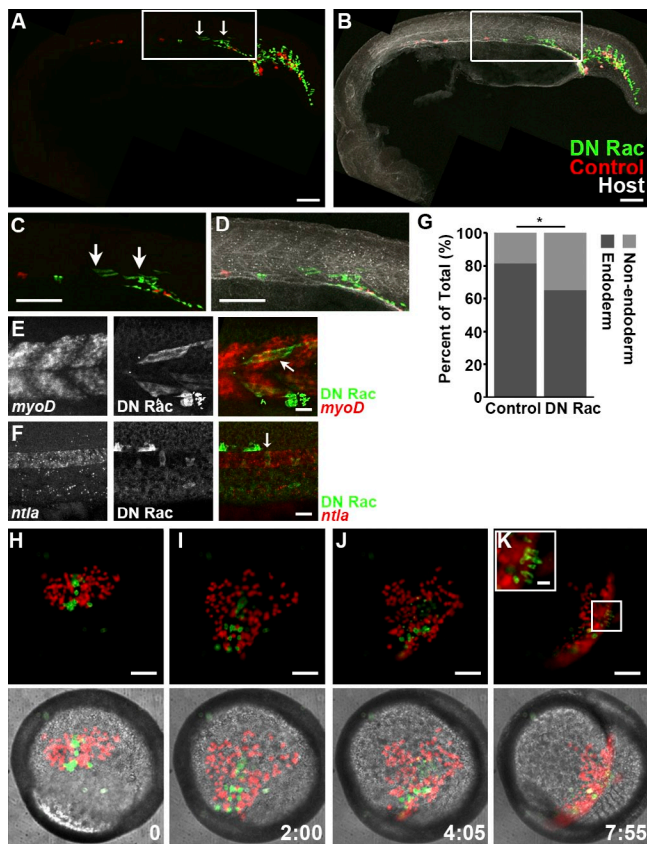


**Figure 7. Cells expressing DN Rac1 are less likely to contribute to endodermal tissues.** (A–D) Lateral view of an embryo 22 h after fertilization containing donor endodermal cells from *Tg(sox17:GFP)* embryos expressing DN Rac1 as well as donor control cells from *Tg(sox17:dsRed)* embryos. Host embryo is labeled with phalloidin. Images in C and D are taken from the boxed regions in A and B, respectively. Arrows point to DN Rac1-expressing cells that appear to aberrantly reside in the somites. Bars, 100  $\mu$ m. (E and F) In situ hybridization analyses of *myoD* (E) or *ntlA* (F) expression show that some DN Rac1-expressing donor cells (arrows) express markers for muscle (E) or notochord (F), respectively, despite also being labeled with the *Tg(sox17:GFP)* transgene (green). Bars, 25  $\mu$ m. (G) Quantification of donor cell contribution to endodermal or nonendodermal tissues. Expression of DN Rac1 significantly increased the likelihood of cells contributing to nonendodermal tissues.  $n = 23$  embryos. \*,  $P < 0.05$  by  $\chi^2$  test. (H–K) Frames from a time-lapse video (Video 7) showing the relative movements of control (red) and DN Rac1-expressing cells (green) from mid-gastrulation to early somitogenesis. Numbers indicate hours elapsed. Bars, 100  $\mu$ m. (inset) Enlarged region of the boxed area showing DN Rac1-expressing cells that have migrated into the notochord. Bar, 25  $\mu$ m.

tissues in which they resided (Fig. 7, C–F). To better understand how Rac1-deficient cells became mislocalized to the mesoderm, we performed time-lapse imaging soon after transplantation (Fig. 7 [H–K] and Video 7). We observed that at 75% epiboly, control cells were spread out along the dorsal–ventral and animal–vegetal axes. In contrast, DN Rac1-expressing cells appeared dispersed along the animal–vegetal axis only (Fig. 7 I). As a result, during the switch to dorsally oriented migration beginning at 90% epiboly, the Rac1-deficient cells reached the dorsal end of the embryo first, whereas control cells were still relatively spread out dorsoventrally (Fig. 7 J). Subsequently, we observed some of the dorsal-most Rac1-deficient cells extruding away from their neighbors and taking on an elongated cell shape reminiscent of notochord cells

(boxed region in Fig. 7 K). These experiments suggest that the migration behavior of endodermal cells during gastrulation is important for maintaining endoderm identity.

## Discussion

In this study, we have shown that during gastrulation stages, endodermal cells undergo developmentally regulated changes in migration behavior, which are driven by corresponding changes in actin cytoskeletal dynamics. We have also shown that the increased actin dynamics and random motility of cells during early gastrulation stages depend on Nodal signaling and Rac1 activity. Furthermore, we showed that Nodal signaling induces the expression of the Rac-specific GEF *prex1* and that *Prex1* functions downstream of Nodal signaling to promote random migration at early gastrulation stages. Together, these observations indicate that the early random migration of endodermal cells is driven by Nodal-induced Rac1 activation.

Interestingly, our data also suggest that the transition to directed migration during late gastrulation may not be simply a result of down-regulation of Nodal and/or Rac1 signaling. First, we observed that Rac1 activity increases rather than decreases during late gastrulation (Fig. S4 I). This increase in Rac1 activity may correlate with the onset of *Cxcl12*–*Cxcr4* chemokine signaling (Mizoguchi et al., 2008), which has been reported to signal through Rac1 (Xu et al., 2012). Second, when we examined endodermal cell migration during late gastrulation in Nodal- or Rac1-inhibited embryos, we found that although cell migration was not severely affected, directional persistence was slightly increased (Fig. S4, C and G). This result suggests that Nodal-dependent signals may still be operating to promote random motility, but, at late stages, they are now superseded by directional cues provided by putative chemoattractants such as *Cxcl12*. Therefore, we propose a model in which Nodal, via *Prex1*, induces global Rac1 activation, which results in directionally random cell migration during early gastrulation stages. Then, as endodermal cells become responsive to directional cues during late gastrulation, these cues may lead to strongly polarized Rac1 activation that overwhelms the Nodal-dependent global Rac1 activation, leading to highly persistent, dorsal-directed migration. Thus, we speculate that by promoting global Rac1 activation, the function of Nodal/*Prex1* during early gastrulation stages is to generate noise in the subcellular distribution of activated Rac1, ensuring that endodermal cells do not inappropriately respond to weak directional cues that may be present at these stages (perhaps guiding mesodermal cell migration). Our observations that loss of Nodal or Rac1 signaling during early gastrulation stages leads to increased directional persistence could be a result of the unmasking of these weak polarization signals that would normally be overwhelmed by the global Rac1 activity induced by high Nodal signaling at these early stages. This model is also consistent with our cell transplantation results in which precociously inducing persistent migration by DN Rac1 expression results in the mistargeting of endodermal cells to mesodermal tissues. Notably, our observations differ from cell culture studies in which decreasing Rac1 activity was sufficient to switch cells from random to persistent migration (Pankov et al., 2005).

Although such a simple signaling mechanism may indeed be sufficient to regulate migratory behaviors under basic cell culture conditions, our results illustrate the complexity of regulating cell migration in the dynamic environment of the developing embryo.

The best-characterized role for Nodal signaling during endoderm development has been the induction of endoderm-specific transcription factor genes. Although it has been previously suggested that Nodal may regulate cell movement (Yokota et al., 2003; Pézeron et al., 2008), the mechanisms by which Nodal could affect cell motility were unknown. Here, we have shown that inhibition of Nodal signaling not only slowed cell migration velocity and increased migration persistence but also suppressed actin dynamics and Rac1 activity. We have further identified the Rac-GEF Prex1 as a downstream target of Nodal signaling. Rac1 is a well-known regulator of actin polymerization and cell migration both in vitro (Gardiner et al., 2002; Srinivasan et al., 2003; Pankov et al., 2005; Woo and Gomez, 2006) and in vivo (Li et al., 2002; Kardash et al., 2010; Yoo et al., 2010), and it has also recently been shown to be crucial for the cell movements underlying gastrulation in mouse (Migeotte et al., 2011). Although our results suggest that the Nodal-dependent Rac1 activity we observed is a result of increased expression of Prex1, Rac1 may be activated via a transcription-independent pathway as well. We observed that acute SB-505124 treatment lasting as little as 15 min was sufficient to alter cell migration behavior (Fig. S5). Indeed, other TGF- $\beta$  ligands have been shown to induce both rapid Rho GTPase activation that is Smad independent as well as sustained increases in Rho activity that involve gene transcription (Kardassis et al., 2009). It is also very likely that other cytoskeletal regulatory proteins besides Rac1 are involved in endoderm morphogenesis. Indeed, in our microarray analysis, we identified several genes associated with cell migration and cytoskeletal dynamics as potential targets of Nodal signaling (Fig. S3 A). In addition, a study using a proteomics-based approach identified at least four cytoskeleton-associated proteins that are differentially regulated between mesendodermal and ectodermal cells (Link et al., 2006); one of these proteins, Ezrin, was demonstrated to function during the migration of prechordal plate progenitor cells by regulating membrane protrusion (Diz-Muñoz et al., 2010). Future studies will no doubt identify additional cytoskeletal regulators important for tissue morphogenesis and organ development.

In this study, we provide evidence that *prex1* is transcriptionally regulated by Nodal signaling. However, GEFs are also subject to posttranscriptional regulation. Although most GEFs are regulated by phosphorylation (Rossman et al., 2005), Prex1 is synergistically activated by PIP<sub>3</sub> and G $\beta\gamma$  (Welch et al., 2002; Barber et al., 2007; Zhao et al., 2007). In neutrophils, Prex1 is thought to act as a coincidence detector that allows for high levels of Rac activation when both second messengers are generated (Weiner, 2002), as occurs when G-protein-coupled chemokine receptors are activated (Stephens et al., 1997). Zebrafish endodermal cells also express chemokine receptors, primarily Cxcr4a (Mizoguchi et al., 2008; Nair and Schilling, 2008). SDF-1-Cxcr4 signaling in primordial germ cells was recently shown to activate Rac1 in a G $\beta\gamma$ -dependent manner

(Xu et al., 2012), making it very likely that Prex1 lies directly in this signaling pathway. However, in terms of endoderm development, several questions remain about the role of Prex1. First, to what extent are both PIP<sub>3</sub> and G $\beta\gamma$  necessary for Prex1 function in vivo? Mizoguchi et al. (2008) suggested that phosphoinositide signaling is not highly active in migrating endodermal cells, and it may be possible to activate Prex1 with G $\beta\gamma$  alone, especially under conditions of low PIP<sub>3</sub> concentrations (Welch et al., 2002). If PIP<sub>3</sub> and/or G $\beta\gamma$  are required for full Prex1 activity, are they generated downstream of receptors such as Cxcr4, and, if so, how do those signaling pathways interact with Nodal signaling? Given that most studies of Prex1 to date have used neutrophils in culture, the developing zebrafish endoderm may represent a useful system to probe important questions about Prex1 function in vivo.

In the double transplantation experiments, we observed that some cells in which random migration was suppressed by DN Rac1 expression seemed unable to maintain endodermal identity and instead contributed to mesodermal tissues. Although we interpret these results as being a result of the suppression of random migration during early gastrulation, it is also possible that DN Rac1 impairs cell movements before gastrulation, such as epiboly and ingression, which could aberrantly place cells in the mesodermal layer. However, although we did observe some endodermal cells that apparently failed to ingress in Prex1 MO-injected embryos, we did not see a similar effect with the low-level DN Rac expression used throughout this study, suggesting that pregastrulation movements are relatively unaffected. Thus, based on our time-lapse analyses, we propose that DN Rac1 expression precociously induces persistent migration, causing cells to more efficiently reach the dorsal side of the embryo. Once there, they may inappropriately interact with mesodermal cells or mesoderm differentiation signals. It is also possible that Rac1 is required for later aspects of endoderm morphogenesis, such as cell-cell adhesion during endodermal sheet formation, which may also affect the ability of Rac-deficient cells to remain within the endoderm.

The ability of cells to switch their migratory behavior has been observed in many different cell types and model systems (Bak and Fraser, 2003; Wolf et al., 2003; Pankov et al., 2005; Pézeron et al., 2008; Sanz-Moreno et al., 2008). In general, it is thought that random migration plays either a dispersive or exploratory role, whereas persistent migration promotes rapid and efficient translocation. The need for multiple modes of migration may be crucial not only during development but in the adult as well. Most notably, processes such as wound healing and axon regeneration require cells to switch from a stationary state to a migratory one. Additionally, different types of invasive tumor cells are characterized by different migratory behaviors (Madsen and Sahai, 2010); some cells are even able to switch between multiple migration modes (Sanz-Moreno et al., 2008), which can impact the efficacy of drugs meant to block metastasis (Wolf et al., 2003; Micuda et al., 2010). Therefore, the findings presented in this study have clear implications beyond developmental processes.

## Materials and methods

### Zebrafish strains and generation of *Tg(sox17:GFP-UTRN)*

Adult zebrafish were maintained under standard laboratory conditions. *Tg(sox17:GFP)<sup>870</sup>* and *Tg(sox17:dsRed)<sup>903</sup>* have been previously described (Chung and Stainier, 2008; Mizoguchi et al., 2008); a 5.0-kb region of the *sox17* gene promoter drives expression of GFP or dsRed. *Tg(sox17:GFP-UTRN)<sup>944</sup>* was generated using components from the Gateway Tol2kit (C.-B. Chien, University of Utah, Salt Lake City, UT; Kwan et al., 2007). The actin-binding domain of human *Utrophin* was amplified by PCR from pCS2-GFP-utrophin (W. Bement, University of Wisconsin, Madison, WI), and BP recombination with pDONR-P3-PR1 generated the entry vector p3E-UTRN. The p5E-*sox17* entry vector was generated by excising a 5.2-kb fragment of the *sox17* promoter from pGFP-*sox17* (Mizoguchi et al., 2008) with PstI and AgeI and blunt-end ligating this fragment into an SmaI site of p5E-MCS. LR recombination among p5E-*sox17*, pME-eGFP-no-stop, p3E-UTRN, and pDEST-Tol2pA2 generated the construct pDEST-Tol2pA2;*sox17:GFP-UTRN*. This construct was used to generate the *Tg(sox17:GFP-UTRN)<sup>944</sup>* line using standard transgenesis protocols.

### Time-lapse microscopy

For time-lapse imaging, dechorionated embryos were embedded in 1% low-melting agarose within glass-bottom Petri dishes (MatTek Corporation). Fluorescent images were acquired on a microscope (Ti-E; Nikon) equipped with a spinning-disk confocal unit (CSU-22; Yokogawa Corporation of America), a charge-coupled device camera (Evolve; Photometrics), and running Micro-Manager software. The microscope stage was enclosed in a temperature-controlled case, and samples were kept at 28.5°C. Unless otherwise specified, time-lapse videos were acquired from the lateral marginal zone, with the embryonic shield oriented to the right. To image overall cell migration (persistence and velocity), z stacks of 4- $\mu$ m intervals were acquired every 30 s with a 20 $\times$ /0.75 NA objective. To image lamellipodia dynamics, z stacks of 4- $\mu$ m intervals were acquired every 5 s with a 20 $\times$ /0.75 NA objective with 1.5 $\times$  zoom. To image retrograde flow, z stacks of 2- $\mu$ m intervals were acquired every 5 s with a 40 $\times$ /1.15 NA objective.

### Image analysis, statistics, and image processing

Image analysis was performed using ImageJ software (National Institutes of Health). All measurements were made from maximum projections of spinning-disk confocal z stacks. Instantaneous velocity and cell position were measured using the Manual Tracking plugin. The persistence index was calculated by dividing the total distance traveled by the net distance traveled. Circularity was determined using the built-in circularity calculations in ImageJ, which uses this formula: circularity =  $4\pi(\text{area}/\text{perimeter}^2)$ . Lamellipodial lifetime was measured using the MTrack2 plugin. Lamellipodia were classified as oriented in the dorsal, ventral, animal, or vegetal directions by the user. Kymographs for retrograde flow measurements were generated along 1-pixel-wide user-defined lines placed within lamellipodial protrusions approximately perpendicular to the direction of protrusion. Analysis was restricted to protrusions that were oriented in the direction of cell migration.

Statistical analysis was performed using GraphPad software. Data presented in bar graphs represent mean  $\pm$  SEM. Unless otherwise noted, p-values were calculated by Student's *t* test, and  $P < 0.05$  was considered significant.

For all figures, images were processed in Photoshop (Adobe) as follows: brightness levels were adjusted, converted to 8-bit depth, and cropped. For Videos 1 and 2 and Videos 8 and 9, images were deconvolved using Huygens Essential software. For Videos 3–5, time-lapse images were denoised in collaboration with J. Sedat (University of California, San Francisco, San Francisco, CA) with software developed by J. Boulanger (Institut de Recherche en Informatique et Systèmes Aléatoires, Rennes, France; Kervrann and Boulanger, 2006).

### RNA expression constructs and MOs

mRNAs and MOs were injected at the one- or two-cell stage. Capped messenger RNA was synthesized using the mMESSAGE mMACHINE kit (Ambion). The following expression plasmids were used in this study: N-terminally myc-tagged human DN (N17) Rac1 in pCS2 (pCS2-myc-DN-Rac1; Woo and Gomez, 2006), full-length zebrafish *sox32* in pCS2 (pCS2-*sox32*; Chung and Stainier, 2008), and TagRFP-PBD in pCS2 (Miller and Bement, 2009). pCS2-mCherry-Prex1 was generated by PCR amplification of the *prex1* ORF, which was cloned into pCS2-N'mCherry (Burkel et al., 2007). The Prex1 MO was designed to target the translation initiation site and was used at 1 ng (5'-CCTCCTCAGTGTATTTCGCT-CAT-3'; synthesized by Gene Tools, LLC).

### *prex1* in situ hybridization

To generate the *prex1* in situ probe, the *prex1* ORF was cloned into pCR-Blunt II-TOPO (Invitrogen). For probe synthesis, pCR-Blunt II-TOPO-*prex1* was digested by SpeI and in vitro transcribed with T7. For in situ hybridization, embryos at 70% epiboly were dechorionated and fixed in 4% PFA overnight at 4°C. Embryos were sunk in 30% sucrose, embedded in optimal cutting temperature medium, and cryosectioned (12  $\mu$ m thick). After drying, sections were fixed in 4% PFA for 10 min at room temperature. Sections were then acetylated with 0.1 M triethanolamine, 2.1 mM HCl, and 0.25% acetic anhydride for 10 min at room temperature. Sections were permeabilized with 1% Triton X-100 in 1 $\times$  PBS for 30 min at room temperature. Nonspecific binding was blocked by incubating sections in hybridization buffer (50% formamide, 5 $\times$  SSC, 0.1% Tween 20, 50 mg/ml heparin, and 500 mg/ml tRNA, pH 6.0) for 4 h at room temperature in a humidified chamber. The *prex1* probe was diluted to 200 ng/ml in hybridization buffer, and sections were incubated overnight at 65°C. Sections were then washed once with 5 $\times$  SSC at 65°C, twice with 0.2 $\times$  SSC at 65°C, and then transferred to room-temperature TBS (100 mM Tris HCl, pH 7.5, and 150 mM NaCl). Sections were blocked for 1 h at room temperature in 2% blocking reagent (Roche). Antidigoxigenin antibody (Roche) was diluted 1:5,000 in 2% blocking reagent, and sections were incubated overnight at room temperature. Sections were washed every 30 min for 4 h with TBS and then equilibrated for 5 min in NTM buffer (100 mM Tris HCl, pH 9.5, 100 mM NaCl, and 5 mM MgCl<sub>2</sub>). Sections were stained with NBT/BCIP solution (1:50 in NTM buffer; Roche) overnight at room temperature. After brief fixation with 4% PFA, sections were air dried overnight at room temperature and then washed twice with xylene. Sections were mounted in Permount (Thermo Fisher Scientific) and imaged on a microscope (Axioplan; Carl Zeiss) with a 20 $\times$ /0.75 NA objective lens.

### Rac1 activity assay

pCS2-TagRFP-PBD was generated by replacing the GFP coding sequence of pCS2-GFP-PBD (Miller and Bement, 2009) with TagRFP (Evrogen). Mosaic expression of TagRFP-PBD was accomplished using established cell transplantation techniques (Stafford et al., 2006; Chung and Stainier, 2008). *Tg(sox17:GFP)<sup>870</sup>* donor embryos were injected with 200 pg *TagRFP-PBD* mRNA, 300 pg *sox32* mRNA, and 2  $\mu$ g A647-dextran (10,000 molecular weight; Invitrogen). At sphere stage, donor cells were transplanted to the marginal zone of isochronic unlabeled host embryos. At 30% epiboly, embryos were treated with 0.5% DMSO or 50  $\mu$ M SB-505124 (Sigma-Aldrich). At shield stage, embryos were embedded in 1% low-melting agarose and imaged by spinning-disk confocal microscopy using a 20 $\times$ /0.75 NA objective with 1.5 $\times$  zoom. Z stacks were acquired at 4- $\mu$ m intervals. Image processing and analysis were performed using ImageJ software. The GFP channel was used as a reference to ensure that only endodermal cells were included for analysis. For the TagRFP-PBD and A647-dextran channels, maximum projections were made, background was set to NaN (not a number), and images were normalized to their own median value. Then, the TagRFP-PBD image was divided by the A647-dextran image to generate a ratiometric image. The mean PBD/dextran ratio was calculated by drawing user-defined regions of interest (ROIs) around cells in the ratiometric images and measuring the mean gray value. Using the same ROIs, we determined the cell area with ratio  $>1.0$  by thresholding the ratiometric images to include pixel values  $>1.0$  and measuring the area occupied by thresholded pixels within each cell.

### Cell transplantations

Cell transplantations were performed as previously described (Stafford et al., 2006; Chung and Stainier, 2008). For double transplantation experiments (Fig. 7), control endodermal donor cells were generated by injecting *Tg(sox17:dsRed)<sup>903</sup>* embryos with 300 pg *sox32* mRNA. Rac1-deficient donor cells were generated by injecting *Tg(sox17:GFP)<sup>870</sup>* embryos with 300 pg *sox32* and 2.5 pg DN Rac1 mRNA. At 4–5 h after fertilization, cells from both control and DN Rac1-expressing donor embryos were transplanted simultaneously to the marginal zone of an unlabeled wild-type host embryo of the same stage. At 22–24 h after fertilization, embryos were imaged on a confocal microscope (LSM 5; Carl Zeiss) with a 20 $\times$ /0.75 NA objective lens, and z stacks were acquired at 2- $\mu$ m intervals. Maximum projections were generated and analyzed using ImageJ software. Measurements were restricted to the trunk region along the yolk extension to exclude the *sox17*-positive dorsal forerunner derivatives. User-defined ROIs were drawn around the gut tube (endodermal), the rest of the trunk dorsal to the gut tube (nonendodermal), and the entire trunk region (total). We measured the area occupied by GFP- or dsRed-positive cells within each ROI and then divided the endodermal or nonendodermal area by the area measured within the total ROI to calculate the percentage of contribution to endodermal or nonendodermal tissues.

Table 1. List of primers used for qPCR

Gene	GenBank/EMBL/DBJ accession no.	Sequence
<i>ef1a</i>	NM_131263	5'-CAAGAAGAGTAGTACCGCTAGCAT-3' 5'-CACGGTGACAACATGCTGGAG-3'
<i>lft2</i>	NM_130961	5'-TGGAGTTACAGTTGCCCTGGGAT-3' 5'-ACAGGATCCAAAGGGAAACACC-3'
<i>prex1</i>	XM_694535	5'-TAAAGGCGGCATCTGGTCCATT-3' 5'-TTGATGCAGACCATGGACCTCAT-3'
<i>tiam1</i>	XM_001924009	5'-TCCCTCAGGATGGAATGAACAGT-3' 5'-GAGGTCAGAATTTGAAGGGAGACC-3'
<i>arhgef25b</i>	XM_692957	5'-CGGAGAATGAATTTTTCGAACTCCAT-3' 5'-GGCTTTCCCTGCCAGGATAC-3'

For in situ hybridization, DN Rac1-expressing *Tg(sox17:GFP)* cells were transplanted into wild-type host embryos at 4–5 h after fertilization, which were then fixed at 22–24 h after fertilization. Whole-mount in situ hybridization for *myoD* and *ntla* was performed as previously described (Thisse and Thisse, 2008). In brief, fixed embryos were dehydrated in methanol at  $-20^{\circ}\text{C}$  overnight. After rehydration, embryos were hybridized with 100 ng/ $\mu\text{l}$  riboprobe in hybridization buffer overnight at  $65^{\circ}\text{C}$ . Excess probe was removed with graded SSC washes. Antidigoxigenin antibody was used at 1:10,000 (Roche) and developed with Fast Red (Roche). Embryos were imaged by confocal microscopy, as described above.

For time-lapse imaging, wild-type donor embryos were injected with 300 pg *sox32* mRNA and 2  $\mu\text{g}$  tetramethylrhodamine-dextran (10,000 molecular weight; Sigma-Aldrich) as a control or with 300 pg *sox32* mRNA, 2.5 pg *DN Rac1* mRNA, and 2  $\mu\text{g}$  FITC-dextran (10,000 molecular weight; Sigma-Aldrich). Cells were transplanted at sphere stage, as described in the previous section. At shield stage, embryos were embedded in 1% low-melting agarose and imaged on a widefield fluorescence microscope (Z.1; Carl Zeiss) with a 5x objective lens. Images were acquired every 5 min. Analysis was restricted to host embryos containing laterally incorporated donor cells.

#### Microarray analysis

To identify endodermally enriched transcripts, endodermal cells were isolated at 70% epiboly by transferring *Tg(sox17:GFP)* embryos to  $\text{Ca}^{2+}$ -free Ringer's solution followed by mechanical disruption with a P200 pipette tip. Dissociated cells were collected by centrifugation and resuspended in  $\text{Ca}^{2+}$ -free Ringer's, and GFP-positive endodermal cells were separated from nonfluorescent nonendodermal cells by FACS. RNA was extracted from both populations using the RNAqueous-Micro Kit (Ambion). cDNAs were amplified, labeled with Cy3 (from endodermal cells) or Cy5 (from nonendodermal cells), and hybridized to the Zebrafish Gene Expression Microarray (V2; microarray services were performed by MOgene, LC using a preprinted Agilent Technologies array). To examine gene expression under Nodal-inhibited conditions, *Tg(sox17:GFP)* embryos were treated at 5 h after fertilization with 50  $\mu\text{M}$  SB-505124 (Sigma-Aldrich) or 0.5% DMSO. For Nodal-activated conditions, *Tg(sox17:GFP)* embryos were injected at the one-cell stage with 2 ng *taram-a\** mRNA or 2 ng *mCherry* mRNA as a control. GFP-positive endodermal cells were isolated by FACS at 70% epiboly, and total RNA was extracted using the RNAqueous-Micro Kit. cDNAs were amplified, labeled with Cy3 (DMSO or *mCherry*) or Cy5 (SB-505124 or *taram-a\**), and hybridized to the Agilent Zebrafish Gene Expression Microarray (V2). The extracted data were normalized and quality controlled using GeneSpring GX software (Agilent Technologies).

#### Real-time quantitative PCR

To examine gene expression under Nodal-inhibited conditions, wild-type embryos were treated at 5 h after fertilization with 50  $\mu\text{M}$  SB-505124 (Sigma-Aldrich) or 0.5% DMSO. For Nodal-activated conditions, wild-type embryos were injected at the one-cell stage with 2 ng *taram-a\** mRNA or 2 ng *mCherry* mRNA as a control. Expression of *lefty2*, a known Nodal target gene, was used to confirm Nodal inhibition and activation (Fig. S3 B). At 70% epiboly, total RNA was extracted using the RNAqueous-Micro Kit, and 1 ng was used for reverse transcription with the SuperScript VILO cDNA Synthesis Kit (Invitrogen). The quantitative PCR reaction mixture contained 2  $\mu\text{l}$  of 10-fold diluted cDNA, 12.5  $\mu\text{l}$  SYBR green PCR master mix (Applied Biosystems), 714 nM of each primer, and nuclease-free water to a total volume of 25  $\mu\text{l}$  in 48-well plates (Illumina). Reactions were performed in the Eco Real-Time PCR System (Illumina, Inc.) as follows: initial

activation at  $95^{\circ}\text{C}$  for 10 min followed by 40 cycles of 30 s at  $95^{\circ}\text{C}$ , 30 s at  $60^{\circ}\text{C}$ , and 30 s at  $68^{\circ}\text{C}$ . Once the PCR was completed, a melt-curve analysis was performed to determine reaction specificity. Samples were run in duplicate, and data presented in Figs. 5 A and S3 B represent means from three independent reactions. The housekeeping gene *ef1a* was used as a reference. Table 1 lists the primers used in this study.

#### Online supplemental material

Fig. S1 shows *sox17* and *sox32* expression in SB-505124-treated embryos and embryos expressing DN Rac1. Fig. S2 shows analysis of migratory behaviors of transplanted endodermal cells as well as the migratory parameters of transplanted DN Rac1 cells. Fig. S3 lists candidate cytoskeletal and migration-related Nodal target genes identified by microarray analysis and shows changes in expression of *lft2*, *tiam1*, and *arhgef25b* in response to Nodal signaling. Fig. S4 shows the effects of Nodal or Rac1 inhibition on endoderm migration at late gastrulation and compares levels of Rac1 activity between early and late gastrulation. Fig. S5 shows the effects of acute Nodal inhibition on endoderm migration. Videos 1 and 2 depict actin dynamics at early and late gastrulation, respectively. Video 3 depicts the switch from random to oriented migration during gastrulation. Video 4 shows the initiation of collective migration and endodermal sheet formation. Video 5 shows the effects of Nodal inhibition on endodermal cell migration. Video 6 shows dynamic Rac1 activity in migrating endodermal cells. Video 7 shows the migration of transplanted control and DN Rac1-expressing cells from 75% epiboly to early somitogenesis. Videos 8 and 9 are z stacks through control and Prex1 MO-injected embryos, respectively. Online supplemental material is available at <http://www.jcb.org/cgi/content/full/jcb.201203012/DC1>.

We thank A. Ayala and M. Alva for fish care, K. Thorn and A. Thwin at the Nikon Imaging Center at University of California San Francisco for access to and assistance with the spinning-disk confocal microscope and deconvolution software, and J. Tollkuhn and R. Arnaout for help with in situ hybridization on embryo sections. We also thank H. Bourne and A. Reade for critical comments on the manuscript.

S. Woo was supported by National Institutes of Health grants T32HL007731 and K01DK092312. M.P. Housley was supported by the California Institute for Regenerative Medicine (grant no. TG2-01153). O.D. Weiner was supported by National Institutes of Health grant GM084040. This work was supported in part by grants from the National Institutes of Health (DK60322) and the Packard Foundation to D.Y.R. Stainier.

Submitted: 5 March 2012

Accepted: 1 August 2012

## References

- Alexander, J., and D.Y. Stainier. 1999. A molecular pathway leading to endoderm formation in zebrafish. *Curr. Biol.* 9:1147–1157. [http://dx.doi.org/10.1016/S0960-9822\(00\)80016-0](http://dx.doi.org/10.1016/S0960-9822(00)80016-0)
- Bak, M., and S.E. Fraser. 2003. Axon fasciculation and differences in midline kinetics between pioneer and follower axons within commissural fascicles. *Development.* 130:4999–5008. <http://dx.doi.org/10.1242/dev.00713>
- Barber, M.A., S. Donald, S. Thelen, K.E. Anderson, M. Thelen, and H.C. Welch. 2007. Membrane translocation of P-Rex1 is mediated by G protein betagamma subunits and phosphoinositide 3-kinase. *J. Biol. Chem.* 282:29967–29976. <http://dx.doi.org/10.1074/jbc.M7101877200>

- Batchelder, E.L., G. Hollopeter, C. Campillo, X. Mezanges, E.M. Jorgensen, P. Nassoy, P. Sens, and J. Plastino. 2011. Membrane tension regulates motility by controlling lamellipodium organization. *Proc. Natl. Acad. Sci. USA*. 108:11429–11434. <http://dx.doi.org/10.1073/pnas.1010481108>
- Burkel, B.M., G. von Dassow, and W.M. Bement. 2007. Versatile fluorescent probes for actin filaments based on the actin-binding domain of utrophin. *Cell Motil. Cytoskeleton*. 64:822–832. <http://dx.doi.org/10.1002/cm.20226>
- Chrzanowska-Wodnicka, M., and K. Burridge. 1996. Rho-stimulated contractility drives the formation of stress fibers and focal adhesions. *J. Cell Biol.* 133:1403–1415. <http://dx.doi.org/10.1083/jcb.133.6.1403>
- Chung, W.S., and D.Y. Stainier. 2008. Intra-endodermal interactions are required for pancreatic beta cell induction. *Dev. Cell*. 14:582–593. <http://dx.doi.org/10.1016/j.devcel.2008.02.012>
- Diz-Muñoz, A., M. Krieg, M. Bergert, I. Ibarlucea-Benitez, D.J. Muller, E. Paluch, and C.P. Heisenberg. 2010. Control of directed cell migration in vivo by membrane-to-cortex attachment. *PLoS Biol.* 8:e1000544. <http://dx.doi.org/10.1371/journal.pbio.1000544>
- Feldman, B., M.A. Gates, E.S. Egan, S.T. Dougan, G. Rennebeck, H.I. Sirotkin, A.F. Schier, and W.S. Talbot. 1998. Zebrafish organizer development and germ-layer formation require nodal-related signals. *Nature*. 395:181–185. <http://dx.doi.org/10.1038/26013>
- Gardiner, E.M., K.N. Pestonjamas, B.P. Bohl, C. Chamberlain, K.M. Hahn, and G.M. Bokoch. 2002. Spatial and temporal analysis of Rac activation during live neutrophil chemotaxis. *Curr. Biol.* 12:2029–2034. [http://dx.doi.org/10.1016/S0960-9822\(02\)01334-9](http://dx.doi.org/10.1016/S0960-9822(02)01334-9)
- Hagos, E.G., and S.T. Dougan. 2007. Time-dependent patterning of the mesoderm and endoderm by Nodal signals in zebrafish. *BMC Dev. Biol.* 7:22. <http://dx.doi.org/10.1186/1471-213X-7-22>
- Kardash, E., M. Reichman-Fried, J.L. Maître, B. Boldajipour, E. Papisheva, E.M. Messerschmidt, C.P. Heisenberg, and E. Raz. 2010. A role for Rho GTPases and cell-cell adhesion in single-cell motility in vivo. *Nat. Cell Biol.* 12:47–53; suppl pp 1–11. <http://dx.doi.org/10.1038/ncb2003>
- Kardassis, D., C. Murphy, T. Fotsis, A. Moustakas, and C. Stouraras. 2009. Control of transforming growth factor beta signal transduction by small GTPases. *FEBS J.* 276:2947–2965. <http://dx.doi.org/10.1111/j.1742-4658.2009.07031.x>
- Kervrann, C., and J. Boulanger. 2006. Optimal spatial adaptation for patch-based image denoising. *IEEE Trans. Image Process.* 15:2866–2878. <http://dx.doi.org/10.1109/TIP.2006.877529>
- Kozma, R., S. Ahmed, A. Best, and L. Lim. 1995. The Ras-related protein Cdc42Hs and bradykinin promote formation of peripheral actin microspikes and filopodia in Swiss 3T3 fibroblasts. *Mol. Cell Biol.* 15:1942–1952.
- Kraynov, V.S., C. Chamberlain, G.M. Bokoch, M.A. Schwartz, S. Slabaugh, and K.M. Hahn. 2000. Localized Rac activation dynamics visualized in living cells. *Science*. 290:333–337. <http://dx.doi.org/10.1126/science.290.5490.333>
- Kwan, K.M., E. Fujimoto, C. Grabber, B.D. Mangum, M.E. Hardy, D.S. Campbell, J.M. Parant, H.J. Yost, J.P. Kanki, and C.B. Chien. 2007. The Tol2kit: A multisite gateway-based construction kit for Tol2 transposon transgenesis constructs. *Dev. Dyn.* 236:3088–3099. <http://dx.doi.org/10.1002/dvdy.21343>
- Li, Z., C.D. Aizenman, and H.T. Cline. 2002. Regulation of rho GTPases by crosstalk and neuronal activity in vivo. *Neuron*. 33:741–750. [http://dx.doi.org/10.1016/S0896-6273\(02\)00621-9](http://dx.doi.org/10.1016/S0896-6273(02)00621-9)
- Lim, J.I., M. Sabouri-Ghomi, M. Machacek, C.M. Waterman, and G. Danuser. 2010. Protrusion and actin assembly are coupled to the organization of lamellar contractile structures. *Exp. Cell Res.* 316:2027–2041. <http://dx.doi.org/10.1016/j.yexcr.2010.04.011>
- Link, V., L. Carvalho, I. Castanon, P. Stockinger, A. Shevchenko, and C.P. Heisenberg. 2006. Identification of regulators of germ layer morphogenesis using proteomics in zebrafish. *J. Cell Sci.* 119:2073–2083. <http://dx.doi.org/10.1242/jcs.02928>
- Madsen, C.D., and E. Sahai. 2010. Cancer dissemination—lessons from leukocytes. *Dev. Cell*. 19:13–26. <http://dx.doi.org/10.1016/j.devcel.2010.06.013>
- Micuda, S., D. Rösel, A. Ryska, and J. Bräbek. 2010. ROCK inhibitors as emerging therapeutic candidates for sarcomas. *Curr. Cancer Drug Targets*. 10:127–134. <http://dx.doi.org/10.2174/156800910791054202>
- Migeotte, I., J. Grego-Bessa, and K.V. Anderson. 2011. Rac1 mediates morphogenetic responses to intercellular signals in the gastrulating mouse embryo. *Development*. 138:3011–3020. <http://dx.doi.org/10.1242/dev.059766>
- Miller, A.L., and W.M. Bement. 2009. Regulation of cytokinesis by Rho GTPase flux. *Nat. Cell Biol.* 11:71–77. <http://dx.doi.org/10.1038/ncb1814>
- Mizoguchi, T., H. Verkade, J.K. Heath, A. Kuroiwa, and Y. Kikuchi. 2008. Sdf1/Cxcr4 signaling controls the dorsal migration of endodermal cells during zebrafish gastrulation. *Development*. 135:2521–2529. <http://dx.doi.org/10.1242/dev.020107>
- Nair, S., and T.F. Schilling. 2008. Chemokine signaling controls endodermal migration during zebrafish gastrulation. *Science*. 322:89–92. <http://dx.doi.org/10.1126/science.1160038>
- Pankov, R., Y. Endo, S. Even-Ram, M. Araki, K. Clark, E. Cukierman, K. Matsumoto, and K.M. Yamada. 2005. A Rac switch regulates random versus directionally persistent cell migration. *J. Cell Biol.* 170:793–802. <http://dx.doi.org/10.1083/jcb.200503152>
- Petrie, R.J., A.D. Doyle, and K.M. Yamada. 2009. Random versus directionally persistent cell migration. *Nat. Rev. Mol. Cell Biol.* 10:538–549. <http://dx.doi.org/10.1038/nrm2729>
- Pézeron, G., P. Mourrain, S. Courty, J. Ghislain, T.S. Becker, F.M. Rosa, and N.B. David. 2008. Live analysis of endodermal layer formation identifies random walk as a novel gastrulation movement. *Curr. Biol.* 18:276–281. <http://dx.doi.org/10.1016/j.cub.2008.01.028>
- Poulain, M., and T. Lepage. 2002. Mezzo, a paired-like homeobox protein is an immediate target of Nodal signalling and regulates endoderm specification in zebrafish. *Development*. 129:4901–4914.
- Reiter, J.F., Y. Kikuchi, and D.Y. Stainier. 2001. Multiple roles for Gata5 in zebrafish endoderm formation. *Development*. 128:125–135.
- Ridley, A.J., H.F. Paterson, C.L. Johnston, D. Diekmann, and A. Hall. 1992. The small GTP-binding protein rac regulates growth factor-induced membrane ruffling. *Cell*. 70:401–410. [http://dx.doi.org/10.1016/0092-8674\(92\)90164-8](http://dx.doi.org/10.1016/0092-8674(92)90164-8)
- Rossmann, K.L., C.J. Der, and J. Sondek. 2005. GEF means go: Turning on RHO GTPases with guanine nucleotide-exchange factors. *Nat. Rev. Mol. Cell Biol.* 6:167–180. <http://dx.doi.org/10.1038/nrm1587>
- Rottner, K., and T.E. Stradal. 2011. Actin dynamics and turnover in cell motility. *Curr. Opin. Cell Biol.* 23:569–578. <http://dx.doi.org/10.1016/j.cob.2011.07.003>
- Sanz-Moreno, V., G. Gadea, J. Ahn, H. Paterson, P. Marra, S. Pinner, E. Sahai, and C.J. Marshall. 2008. Rac activation and inactivation control plasticity of tumor cell movement. *Cell*. 135:510–523. <http://dx.doi.org/10.1016/j.cell.2008.09.043>
- Shen, X., J. Li, P.P. Hu, D. Waddell, J. Zhang, and X.F. Wang. 2001. The activity of guanine exchange factor NET1 is essential for transforming growth factor-beta-mediated stress fiber formation. *J. Biol. Chem.* 276:15362–15368. <http://dx.doi.org/10.1074/jbc.M009534200>
- Sosa, M.S., C. Lopez-Haber, C. Yang, H. Wang, M.A. Lemmon, J.M. Busillo, J. Luo, J.L. Benovic, A. Klein-Szanto, H. Yagi, et al. 2010. Identification of the Rac-GEF P-Rex1 as an essential mediator of ErbB signaling in breast cancer. *Mol. Cell*. 40:877–892. <http://dx.doi.org/10.1016/j.molcel.2010.11.029>
- Srinivasan, S., F. Wang, S. Glavas, A. Ott, F. Hofmann, K. Aktories, D. Kalman, and H.R. Bourne. 2003. Rac and Cdc42 play distinct roles in regulating PI(3,4,5)P3 and polarity during neutrophil chemotaxis. *J. Cell Biol.* 160:375–385. <http://dx.doi.org/10.1083/jcb.200208179>
- Stafford, D., R.J. White, M.D. Kinkel, A. Linville, T.F. Schilling, and V.E. Prince. 2006. Retinoids signal directly to zebrafish endoderm to specify insulin-expressing beta-cells. *Development*. 133:949–956. <http://dx.doi.org/10.1242/dev.02263>
- Stainier, D.Y. 2002. A glimpse into the molecular entrails of endoderm formation. *Genes Dev.* 16:893–907. <http://dx.doi.org/10.1101/gad.974902>
- Stephens, L.R., A. Eguinoa, H. Erdjument-Bromage, M. Lui, F. Cooke, J. Coadwell, A.S. Smrcka, M. Thelen, K. Cadwallader, P. Tempst, and P.T. Hawkins. 1997. The G beta gamma sensitivity of a PI3K is dependent upon a tightly associated adaptor, p101. *Cell*. 89:105–114. [http://dx.doi.org/10.1016/S0092-8674\(00\)80187-7](http://dx.doi.org/10.1016/S0092-8674(00)80187-7)
- Thisse, C., and B. Thisse. 2008. High-resolution in situ hybridization to whole-mount zebrafish embryos. *Nat. Protoc.* 3:59–69. <http://dx.doi.org/10.1038/nprot.2007.514>
- Waters, J.E., M.V. Astle, L.M. Ooms, D. Balamatsias, R. Gurung, and C.A. Mitchell. 2008. P-Rex1 - a multidomain protein that regulates neurite differentiation. *J. Cell Sci.* 121:2892–2903. <http://dx.doi.org/10.1242/jcs.030353>
- Weiner, O.D. 2002. Rac activation: P-Rex1 - a convergence point for PIP(3) and Gbetagamma? *Curr. Biol.* 12:R429–R431. [http://dx.doi.org/10.1016/S0960-9822\(02\)00917-X](http://dx.doi.org/10.1016/S0960-9822(02)00917-X)
- Welch, H.C., W.J. Coadwell, C.D. Ellison, G.J. Ferguson, S.R. Andrews, H. Erdjument-Bromage, P. Tempst, P.T. Hawkins, and L.R. Stephens. 2002. P-Rex1, a PtdIns(3,4,5)P3- and Gbetagamma-regulated guanine-nucleotide exchange factor for Rac. *Cell*. 108:809–821. [http://dx.doi.org/10.1016/S0092-8674\(02\)00663-3](http://dx.doi.org/10.1016/S0092-8674(02)00663-3)
- Welch, H.C., A.M. Condliffe, L.J. Milne, G.J. Ferguson, K. Hill, L.M. Webb, K. Okkenhaug, W.J. Coadwell, S.R. Andrews, M. Thelen, et al. 2005. P-Rex1 regulates neutrophil function. *Curr. Biol.* 15:1867–1873. <http://dx.doi.org/10.1016/j.cub.2005.09.050>
- Wolf, K., I. Mazo, H. Leung, K. Engelke, U.H. von Andrian, E.I. Deryugina, A.Y. Strongin, E.B. Bröcker, and P. Friedl. 2003. Compensation mechanism in

- tumor cell migration: Mesenchymal–amoeboid transition after blocking of pericellular proteolysis. *J. Cell Biol.* 160:267–277. <http://dx.doi.org/10.1083/jcb.200209006>
- Woo, S., and T.M. Gomez. 2006. Rac1 and RhoA promote neurite outgrowth through formation and stabilization of growth cone point contacts. *J. Neurosci.* 26:1418–1428. <http://dx.doi.org/10.1523/JNEUROSCI.4209-05.2006>
- Wu, Y.I., D. Frey, O.I. Lungu, A. Jaehrig, I. Schlichting, B. Kuhlman, and K.M. Hahn. 2009. A genetically encoded photoactivatable Rac controls the motility of living cells. *Nature.* 461:104–108. <http://dx.doi.org/10.1038/nature08241>
- Xu, H., E. Kardash, S. Chen, E. Raz, and F. Lin. 2012. Gβγ signaling controls the polarization of zebrafish primordial germ cells by regulating Rac activity. *Development.* 139:57–62. <http://dx.doi.org/10.1242/dev.073924>
- Yamada, K.M., and E. Cukierman. 2007. Modeling tissue morphogenesis and cancer in 3D. *Cell.* 130:601–610. <http://dx.doi.org/10.1016/j.cell.2007.08.006>
- Yokota, C., M. Kofron, M. Zuck, D.W. Houston, H. Isaacs, M. Asashima, C.C. Wylie, and J. Heasman. 2003. A novel role for a nodal-related protein; Xnr3 regulates convergent extension movements via the FGF receptor. *Development.* 130:2199–2212. <http://dx.doi.org/10.1242/dev.00434>
- Yoo, S.K., Q. Deng, P.J. Cavnar, Y.I. Wu, K.M. Hahn, and A. Huttenlocher. 2010. Differential regulation of protrusion and polarity by PI3K during neutrophil motility in live zebrafish. *Dev. Cell.* 18:226–236. <http://dx.doi.org/10.1016/j.devcel.2009.11.015>
- Zhao, T., P. Nalbant, M. Hoshino, X. Dong, D. Wu, and G.M. Bokoch. 2007. Signaling requirements for translocation of P-Rex1, a key Rac2 exchange factor involved in chemoattractant-stimulated human neutrophil function. *J. Leukoc. Biol.* 81:1127–1136. <http://dx.doi.org/10.1189/jlb.0406251>
- Zorn, A.M., and J.M. Wells. 2009. Vertebrate endoderm development and organ formation. *Annu. Rev. Cell Dev. Biol.* 25:221–251. <http://dx.doi.org/10.1146/annurev.cellbio.042308.113344>